Soft polymerization of hexamethyldisiloxane by coupling pulsed direct-liquid injections with dielectric barrier discharge

Laura Cacot, Guillaume Carnide, Myrtil L Kahn, Nicolas Naudé, Luc Stafford, Richard Clergereaux

Received: 30 August 2022 | Revised: 4 November 2022 | Accepted: 10 November 2022

DOI: 10.1002/ppap.202200165

RESEARCH ARTICLE

PLASMA PROCESSES AND POLYMERS

Soft polymerization of hexamethyldisiloxane by coupling pulsed direct-liquid injections with dielectric barrier discharge

Laura Cacot[1,2] | **Guillaume Carnide**[2,3] | **Myrtil L. Kahn**[3] | **Nicolas Naudé**[2] | **Luc Stafford**[1] | **Richard Clergereaux**[2]

[1]Département de Physique, Université de Montréal, Montréal, Québec, Canada

[2]LAPLACE, Université de Toulouse, CNRS, INPT, UPS, Toulouse, France

[3]LCC, CNRS (UPR 8241), Université de Toulouse, Toulouse, France

Correspondence
Richard Clergereaux, LAPLACE, Université de Toulouse, CNRS, INPT, UPS, Toulouse, France.
Email: richard.clergereaux@laplace.univ-tlse.fr

Abstract

This work examines the combination of pulsed direct-liquid injections with dielectric barrier discharge at atmospheric pressure for the deposition of organosilicon coatings using hexamethyldisiloxane (HMDSO) as the precursor and nitrogen as the carrier gas. In such conditions, deposition relies on the charging of micrometer droplets and their transport toward the substrate by the Coulomb force. The thin-film morphology and extent of precursor fragmentation are strongly linked to the amount of energy provided by the filamentary discharge to HMDSO droplets. While cross-linked and smooth coatings were achieved at low energies as in standard gas phase plasma polymers, viscous and droplet-like structured thin films were deposited at higher energies. The latter material is attributed to the soft polymerization of HMDSO droplets related to plasma–droplet interactions.

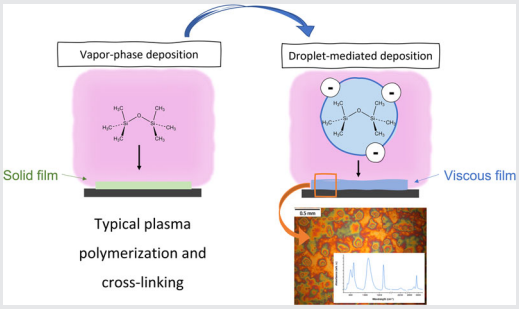

KEYWORDS

aerosols, atmospheric pressure plasma deposition, dielectric barrier discharge, organosilicon coatings, pulsed direct liquid injection, thin films

1 | INTRODUCTION

Thin films obtained from dry processes have garnered great attention due to their wide scope of functionalities.[1-8] For applications requiring low-cost deposition over large areas, atmospheric-pressure plasma processes, including those based on dielectric barrier discharges (DBDs), are relevant.[9-12] In most systems, reactive precursors used for plasma deposition are injected either as gases (e.g. silane) or vapors (e.g. hexamethyldisiloxane [HMDSO]).[13-16] For the

latter, injection of precursor vapors in atmospheric pressure plasma can rely on a carrier gas bubbling in a liquid,[15] direct vaporization using a warm water bath,[17] or a vapor source controller.[18] However, these methods involving gases and vapors can only be used with low precursor flow rates.[19,20] In addition, only volatile and thermally stable precursors can be injected.

Aerosol-assisted methods are relevant alternatives to inject a larger quantity and variety of liquids, regardless of their composition and properties.[8,21] Such processes involve the injection of liquid precursors in the form of droplets with a carrier gas used to transport the aerosol toward the reactor. These methods have been extensively applied in the field of chemical vapor deposition (CVD) and atomic layer deposition (ALD)[22] and has attracted increasing interest in plasma-enhanced chemical vapor deposition (PECVD).[23-30] In addition to single-phase liquid precursors for CVD and PE-CVD, aerosol-assisted methods can also inject multicomponent solutions such as mixtures of liquids, dispersions of nanoparticles or colloidal solutions; such route is then promising to deposit nanocomposite (multi)functional thin films. For example, nanocomposites were produced using a solution of metal (gold) salts dissolved in a polymerizable solvent (isopropanol)[31] or colloidal solutions with metal-oxide (ZnO, TiO_2) nanoparticles injected in low- and atmospheric-pressure plasmas.[12,32-36]

In all studies based on aerosols and plasmas reported in the literature, precursors for thin-film deposition are injected in a continuous way. Depending on the substrate temperature, applied power conditions (continuous or pulsed), reactant partial pressure and flow rate, and location of the substrate along the gas flow lines, the so-called "soft plasma polymerization" (SPP) can be achieved.[37] In such conditions, the plasma can deposit a solid film with a minimal precursor fragmentation such that the deposited coating retains the molecular complexity, functionality, and value of the monomer.[28,29,38–40] The benefits of SPP processes are significant and relatively well documented in the literature, in particular for biomedical applications.[41,42]

Recently, the combination of pulsed direct-liquid injection (DLI) with pulsed DBDs was explored for deposition of organosilicon coatings using HMDSO as the precursor and nitrogen as the carrier gas.[43] This approach offers a wide parameter space for fundamental studies of the so-called misty plasma (combination of liquid, gas, and plasma states)[44] at atmospheric pressure and their application to (multi)functional thin-film deposition. By investigating the effects of process parameters, namely, plasma-on time, delay between HMDSO precursor injection and plasma ignition, and precursor amount on film thickness, it was found that the deposition process results from the charging of micrometer droplets and their transport toward the dielectrics of the DBD cell by the low-frequency electric field.[43,45] In such conditions, the addition of a continuous carrier gas flow to the pulsed HMDSO aerosol significantly reduced the deposition rate due to a prominent decrease of the precursor residence time.[43,46] Finally, it was found that pulsed, aerosol-assisted plasma deposition is limited by the amount of energy provided to precursor droplets and not by precursor insufficiency.[16,43,47–49]

In this study, we examine the physico–chemical structure of such films, in particular, the morphology and the extent of precursor fragmentation. It is demonstrated that these aspects are strongly linked to the amount of energy provided to precursor droplets and that polymers, that is, linear macromolecules with repeating subunits, can be achieved through judicious control of the process conditions. The work is divided into two parts. In the first section, the aerosol-assisted PECVD process is analyzed by injecting a pulsed aerosol of HMDSO without continuous nitrogen carrier gas flow. In the second section, the role of the droplet's residence time is examined through variations of the continuous nitrogen gas flow rate.

2 | EXPERIMENTAL SETUP AND DIAGNOSTICS

As illustrated in Figure 1, the setup used in this work consists of a plane-to-plane DBD and a two-stage pulsed DLI device (Atokit from Kemstream™) for the introduction of HMDSO aerosol with nitrogen carrier gas.[43] The

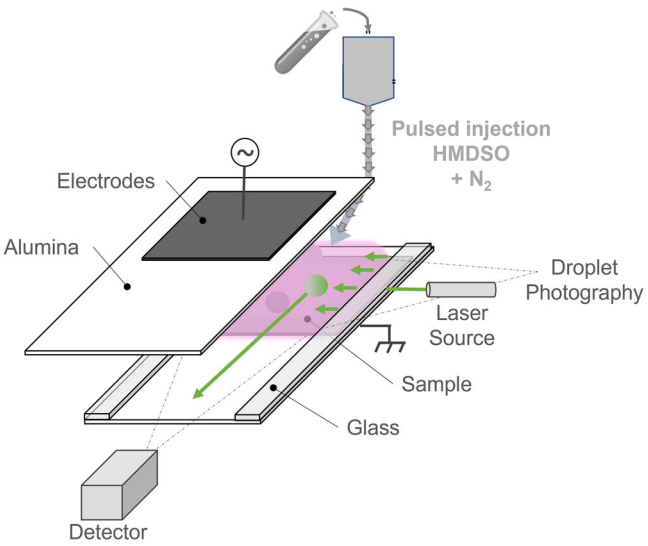

FIGURE 1 Schematic view of the experimental setup coupling pulsed hexamethyldisiloxane (HMDSO) aerosols with dielectric barrier discharges for thin film deposition. The laser source and detector used for droplet scattering measurements are also shown.

apparatus for DBD ignition and charge-current-voltage diagnostics were described in previous publications.[13,50,51] The power injected in the DBD is calculated based on the measured charge and voltage values, with Lissajous figure.[52] Here, the discharge is sustained by the application of a low-frequency sinusoidal voltage (1 kHz, 13 $kV_{peak\ to\ peak}$) between two dielectrics separated by a 1 mm gas gap.

Of note, the plasma chamber is first vacuum pumped to eliminate contaminants, then it is filled with N_2 (Alphagaz 1, Air Liquide) to a pressure of 1 bar. Constant pressure in the chamber is maintained using a self-regulating valve (MKS 248D) that is coupled to a pressure regulation system. In some cases, a nitrogen continuous flow between 0.7 and 1.4 L. min^{-1} is added to the pulsed aerosol. HMDSO (≥ 98%; Sigma Aldrich) is placed in a Fisher-Porter tube plugged to the first stage of the DLI that is pressurized with 2.5 bar absolute N_2 (Alphagaz 1, Air Liquide). The liquid is pulsed injected into a second stage chamber as pulses (5 ms opening time and 0.1 Hz injection frequency), where it is mixed with 2 bar absolute of N_2 (Alphagaz 1, Air Liquide). The mixture is then injected as pulses (10 ms opening time and 0.1 Hz injection frequency) into the gas pipe and diffuser connecting the DLI to the DBD chamber. Over the range of experimental conditions investigated, the HMDSO aerosols injected into the DBD cell consists in a fog of micrometer size droplets[43] and the liquid injection rate is 2.7 μL per pulse, that is, 16.0 μL. min^{-1}.

While this low-frequency DBD operated in nominally pure nitrogen exhibits homogeneous behavior in both current-charge-voltage and optical characteristics,[10] the injection of HMDSO with the DLI induces discharge destabilization and thus a filamentary DBD.[43] In agreement with the literature,[28,29] the average diameter of the filaments observed by fast optical imaging (Princeton Instruments PI-MAX3, 1000 frames per second, not shown here) were in the 200 μm range.

A silicon sample is placed on the bottom dielectric for ex situ measurements of organosilicon thin-film deposition. The morphology is first observed by optical microscopy (OMAX) and analyzed on several images by using ImageJ software (free software: https://imagej.nih.gov/ij/). For each microstructure, two perpendicular sizes, denoted D_1 and D_2, are measured and processed using the 2D size plot method developed by Zhao et al.[53] This approach aims to point out the various types of microstructures on the coating and their shape. Here, it is used to emphasize the isotropic nature of the microstructures formed on the substrate through plasma droplet interactions. The coatings are also analyzed by FTIR spectroscopy (Vertex 70; Bruker®) in transmission mode. The spectra are recorded in the range of 500–4000 cm^{-1}, with a spectral resolution of 4 cm^{-1}. Each spectrum corresponds to the average of 16 scans.

Finally, for selected experimental conditions, laser light scattering measurements are conducted to image the presence of droplets in the discharge cell. To avoid interferences with the emission of a nitrogen plasma, a 532 nm laser is used and installed perpendicular to the gas flow lines (see Figure 1). Light scattering is detected at 90° with respect to the laser beam using a monochromator and a detector centered at 532 nm or imaged on the side of the discharge cell, through a glass spacer.

3 | CHARACTERIZATION OF THE ORGANOSILICON COATINGS DEPOSITED WITHOUT CONTINUOUS NITROGEN CARRIER GAS

Figure 2 depicts typical optical microscope images of the coatings deposited on silicon wafers for 1, 2, and 4 min of plasma treatment without continuous nitrogen carrier gas flow added to the pulsed HMDSO aerosol in nitrogen. As can be seen, the coatings are different from those generally produced in classical N_2 Townsend discharge with HMDSO.[49,54,55]

For 1 min, the image displayed in Figure 2 shows that the coating consists in micrometer spots dispersed on the substrate surface. Moreover, while the films obtained with continuous injection of fully vaporized HMDSO are generally smooth,[56,57] Figure 2 reveals that the ones obtained with pulsed HMDSO injection at longer times are viscous and macroscopically inhomogeneous. After 2 min, a microscale coating with surface irregularities is observed, as suggested by the thin-film interferences. Such iridescence, linked to thin-film thickness variations, are not linked to gradients along the gas flow lines,[58–60] but rather indicates a deposition of droplets as observed for fuel droplets on top of water. Similar droplet-like morphologies were observed by O'Neil et al.[57] in a corona discharge produced in helium at higher HMDSO flow rates (80 μL. min^{-1} vs. 16 μL. min^{-1} in our conditions) using a continuous precursor injection method (vapor source controller). This aspect seems even more prominent after 4 min, with features characterized by much larger dimensions.

Of note, similar coatings and size distributions were observed with the silicon substrate placed on either the top or the bottom dielectric (not shown). This reveals that, over the range of experimental conditions investigated, the top dielectric is not a source of precursor. More precisely, this means that the film deposited on the bottom electrode does not result from an accumulation of matter on the top electrode and its release toward the bottom one by gravity.

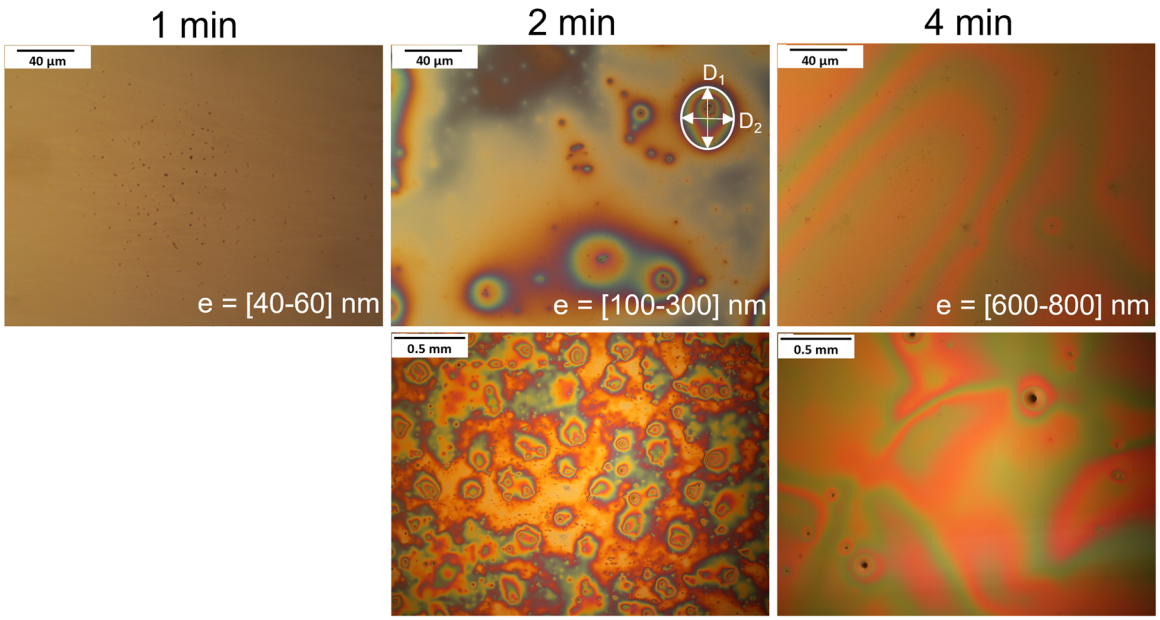

FIGURE 2 Optical microscopy images of the coatings obtained after 1, 2, and 4 min. The results are shown at high (top row) and low (bottom row) magnifications.

It further confirms that the coatings result from HMDSO droplets, and that thin-film deposition occurs following the transport of charged droplets by the low-frequency electrostatic force toward both the top and bottom dielectrics. This force thus plays a very important role in aerosol-assisted plasma deposition processes with respect to other ones such as gravitational, thermophoresis, and dielectrophoresis forces.[43]

The dimensions of the microstructures observed in Figure 2 are extracted by post-processing, and the obtained values are shown in Figure 3 in the form of a typical 2D-plot.[53] Figure 3 clearly shows that the type and the average size of those microstructures vary with plasma deposition time. A single point cloud is observed for the shortest time with size <10 µm. This indicates that for 1 min, the coatings are composed of isotropic structures, with an average diameter of about 1 µm. It is worth mentioning that these microstructures observed for short plasma deposition times cannot be attributed to the impact of filaments on the surface, since their average diameter of about 200 µm[61,62] is much larger than the microstructures observed in the 2D plots (Figure 3). It underlines that the deposit is only made up of droplets with only diameters in the low micrometer scale and below. As a rough estimation, for a steady-state charge of ~10^4 electrons on a 10 µm HMDSO droplet (and thus a mass-to-charge ratio ~10^2 kg/C),[45,50] at 1 kHz, the amplitude of oscillations of the charged droplet in a 4 kV.mm^{-1} electric field (recall that the electric field is linked to the gas gap voltage after discharge breakdown)[63] becomes comparable to the gas gap (~1 mm). Therefore, droplets much smaller than 10 µm are easily collected

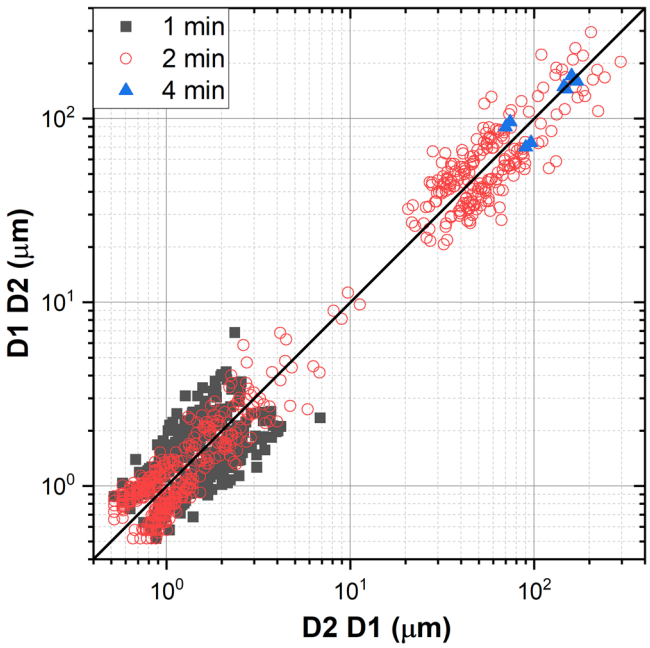

FIGURE 3 2D-plots of the microstructures observed on the substrate after 1, 2, and 4 min of plasma deposition.

within half-period of the applied voltage whereas droplets much larger than 10 µm are trapped in the gas gap by the oscillating electric field.[43]

For the intermediate time, the 2D plot comprising two-point clouds underlines the presence of two populations, one as for short time with size <10 µm and an additional one ranging from 30 up to 300 µm. Finally, for the longest time, only a few points are observed with

value below 10 μm, but most of the microstructures are above 100 μm with a deposit more homogeneous. Since thin-film deposition results from the deposition of charged HMDSO droplets with a dimension of ~1 μm,[43] the presence of larger features indicates droplet association on the substrate surface as discussed in 3D deposition processes.[64] Such association reactions are typically observed during droplet condensation on a hydrophilic surface.[65]

Although the filaments do not directly contribute to the film microstructure, they play an important role in the deposition process at multiple levels. First, the interaction of ions and electrons from the filaments with the aerosol induces HMDSO droplets surface charging over very short time scales (~5 ns with average ion and electron number densities of ~10^{12} cm^{-3} in filamentary discharges operated in nitrogen).[10] Since this charging time is much shorter than (i) the duration of micro-discharges (~100 ns) in filamentary DBDs,[66] (ii) the period of the applied voltage (1 ms at 1 kHz), and (iii) the gas residence times (>3 ms), one can safely assume that all HMDSO droplets become charged. In the absence of continuous gas flow, and thus of a significant neutral drag force, droplets remain between the two electrodes for relatively long-time scales. Since the neutral gas temperature seems insufficient to induce droplet evaporation,[67] numerous filaments-droplets interactions can make the droplet instable and initiate Coulomb fission.[67,68] The result is the formation of smaller droplets that can more easily be transported toward the substrate following their interaction with the low-frequency electric field[43] as observed for short plasma deposition times.

Imaging and light scattering are used to observe the droplet transport following pulsed DLI. A typical picture recorded at 4 min on the side of the DBD cell along the gas flow lines is presented in Figure 4a. Clearly, in addition to the relatively weak background signal, large features can be seen in some spots of the DBD cell by laser scattering, which is consistent with the presence of HMDSO droplets in the gas gap as well as their growth as larger-scale features.[69–72]

The time evolution of the light emission scattered at 90° with respect to the laser beam (see Figure 1) is presented in Figure 4b as a function of plasma deposition time. The first observation is that the intensity progressively increases and reaches a saturation after several pulse injections (the "noise" around the saturation value is attributed to the "local" measurement of the laser beam dimension across the width of the DBD cell). Such temporal evolution of scattered light intensity may be attributed to an increase in the number and/or size of droplets over time. Higher numbers and larger sizes

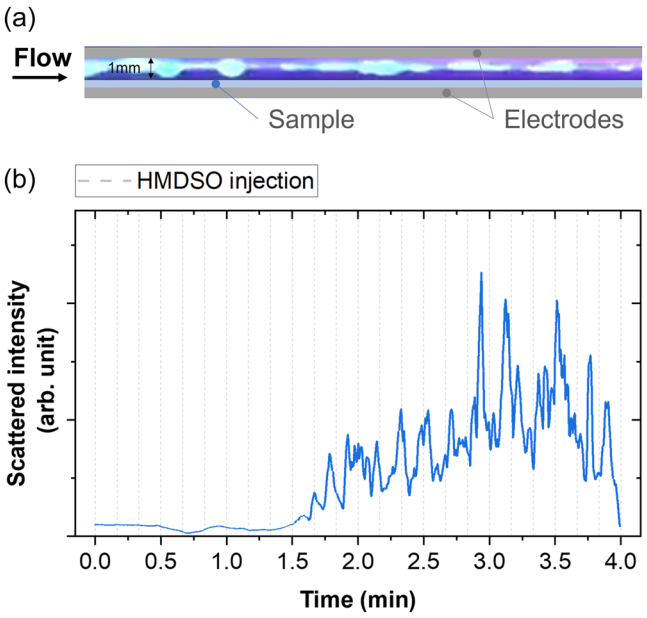

FIGURE 4 (a) Typical laser backscattering image of the gas gap after 4 min of plasma deposition and (b) temporal evolution of the intensity of light scattered at 90° with respect to the laser beam for experiments without continuous gas flow rate.

reveal that the HMDSO droplets injected by the pulsed DLIs are efficiently confined in the plasma region by the electrostatic force. In the absence of a carrier gas flow (and thus with a minimal contribution from the neutral drag force), they can therefore accumulate in the gas gap. Quantitatively, assuming a minimal gas flow of 0.07 $L.min^{-1}$ (without continuous carrier gas flow, this gas flow results from the constant pressure operation in the DBD cell maintained using a self-regulating valve located upstream of the pumping system),[43] the ratio of neutral drag-to-Coulomb force amplitude on 10 μm HMDSO droplets with ~10^4 electrons is only 1%, which is consistent with a significant droplet confinement. In Figure 4b, the presence of the saturation for longer plasma deposition times reveals that the system reaches an equilibrium between (i) the input of HMDSO droplets by pulsed DLI, (ii) the deposition of small-scale droplets on both dielectrics following their transport by the low-frequency electric field, and (iii) the output of large scale HMDSO droplets being confined by the electric field and transported away from the DBD cell by the small neutral drag force.

As indicated in Figure 2, the film thickness measured by stylus profilometry after 1 min of plasma deposition is in the 40–60 nm range. After 2 min, this coating is 2–3 times thicker and after 4 min., the film thickness reaches 600–800 nm. Thin-film deposition rate thus increases from 40 to 60 $nm.min^{-1}$ to 150–200 $nm.min^{-1}$ between 1 and 4 min.; such evolution of the deposition rate is

consistent with 3D island deposition and/or the accumulation of HMDSO droplets in the gas gap observed by laser scattering. Beyond 4 min., no significant change in the thin-film deposition rate was observed, which is consistent with the saturation seen in Figure 4b. Of note, deposition rates in the 150–200 nm.min^{-1} range are among the upper limits for organosilicon coatings using HMDSO in atmospheric pressure plasmas.[10,73]

Considering that thin-film deposition is limited to the discharge region (18 cm^2) due to droplet charging and trapping between the two electrodes, and that the film thickness (600–800 nm) remains relatively homogeneous along the gas flow lines, the process yields after 4 min to a coating of 1.0–1.4 × 10^{-3} cm^3. With a liquid injection rate of 16.0 μL. min^{-1}, and thus a total injection volume of 64.0 μL, the conversion yield of HMDSO droplets into organosilicon thin film (ratio of the coating volume with the liquid injected one) is 1.5–2.2 vol%. This yield confirms that many droplets do not contribute to the film deposition; this results from their trapping in the gas gap over multiple low-frequency cycles before being evacuated out of the DBD cell. Thin-film deposition thus becomes limited by the amount of energy provided to precursor droplets not only for charging, but also for fission to promote the transport of smaller droplets towards the substrate.[43]

Plasma-deposited coatings are further investigated by transmission FTIR spectroscopy. The spectra recorded at the middle of the sample as a function of plasma deposition time are reported in Figure 5a. As a comparison, a FTIR spectrum from liquid HMDSO is also presented. Si-O-Si stretching band detected at 1000–1150 cm^{-1} indicates that the central skeleton of HMDSO is not significantly broken by the discharge. This hypothesis is in good agreement with the CH_3 rocking vibrations in Si-$(CH_3)_3$ at 840 cm^{-1} and the asymmetric and symmetric bending vibrations of CH_x at ~2900 cm^{-1}. Indeed, the main difference between liquid HMDSO and the plasma-deposited film corresponds to the CH_3 rocking vibrations in Si-$(CH_3)_2$ at 800 cm^{-1} as observed in polydimethylsiloxane that suggests weak plasma dissociation as well as soft polymerization. Furthermore, a change in the relative intensity of these two peaks can be observed over time. According to Siliprandi et al.[20] the ratio of these two bands is related to the degree of polymerization: in highly-fragmented deposits, Si-$(CH_3)_2$ relative absorbance increases, while in low-fragmented deposits, there is a high retention of Si-$(CH_3)_3$. Of note, previous studies on plasma polymerized droplet-like coatings with corona discharge in helium[57] do not show either Si-$(CH_3)_3$ nor Si-$(CH_3)_2$ bands in the FTIR spectra suggesting that pulse aerosol plasma processes involve specific plasma deposition mechanisms.

The influence of the plasma deposition time on the Si-$(CH_3)_2$-to-Si-$(CH_3)_3$ band ratio is plotted in Figure 5b. Clearly, even if the thin-film deposition rate increases between 1 and 4 min. (as reported in the inset of

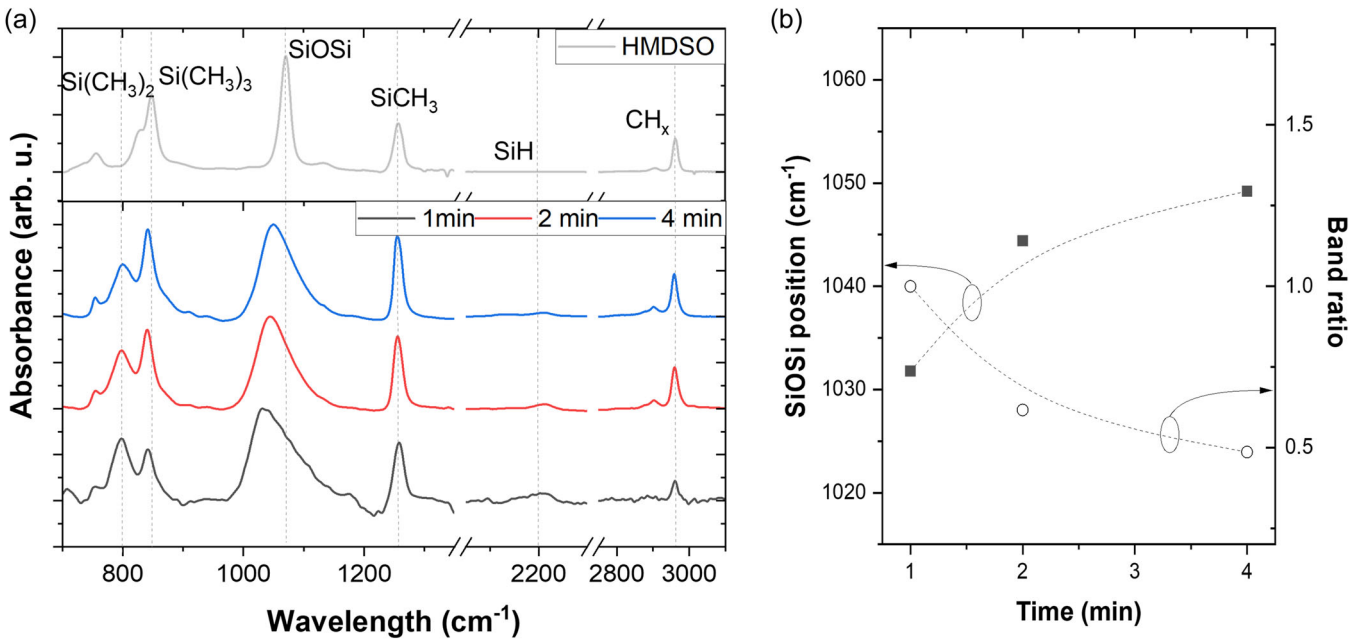

FIGURE 5 (a) FTIR spectra taken in the middle of the sample for various times and compared with the one of liquid hexamethyldisiloxane (HMDSO). (b) On the left scale Si-O-Si peak position and on the right scale degree of polymerization Si-$(CH_3)_2$-to-Si-$(CH_3)_3$ bands ratio) as a function of time.

Figure 2), the degree of polymerization decreases with increasing deposition time, in good agreement with the viscous aspect of the deposited films. Plasma polymerization can also be monitored by plotting the position of the Si-O-Si band observed by FTIR (from 1000 to 1100 cm^{-1}). As can be seen in Figure 5b, an important shift in the position of the Si-O-Si band is observed, from 1032 cm^{-1} at 1 min to almost 1050 cm^{-1} at 4 min. Of note, this latter value approaches the one of liquid HMDSO without plasma polymerization (see Figure 5a). Hence, a large amount of matter probed by transmission FTIR after 4 min of plasma deposition tends toward a polymer formed by linear macromolecules with repeating subunits.[37] The aerosol-assisted process thus consists in a soft polymerization assisted by plasma. On the other hand, early in the process, a higher fragmentation of the monomer is seen, with features typically reported for plasma-polymerized organosilicon coatings with fully vaporized HMDSO.[8,56,57]

4 | CHARACTERIZATION OF THE ORGANOSILICON COATINGS DEPOSITED WITH CONTINUOUS NITROGEN CARRIER GAS

Considering that the thin-film deposition process is strongly influenced by the droplet residence time, plasma polymerization and the deposition of a polymer may be further controlled by varying this parameter. Herein, the residence time of HMDSO droplets in the plasma volume is changed by introducing a continuous flow of nitrogen used as carrier gas into the interelectrode space.

Figure 6 depicts the optical microscope images corresponding to deposits obtained under varying gas flow conditions after 4 min. of plasma treatment. Clearly, the morphology of the plasma-deposited layers varies with a continuous gas flow rate, and the deposits become less "mushy" at higher flow rates. Moreover, while the liquid injection rate remains constant (16 $\mu L.\,min^{-1}$), the film thickness and, consequently, the deposition rate decreases (by about a factor of 2 between 0 and 0.7 $L.\,min^{-1}$). This lower deposition rate at high carrier gas flows was observed in other studies and results from the lower specific energy inputs.[43]

As highlighted in the previous section, the collection of HMDSO droplets on the substrate leading to organosilicon thin-film deposition strongly depends on their motion in the low-frequency electric field.[43] As the flow of continuous nitrogen gas increases, the contribution of the neutral drag force increases such that the transport of droplets along the gas flow lines becomes more important, that is, that their residence time decreases. Quantitatively, the ratio of neutral drag-to-Coulomb force amplitude on 10 μm HMDSO droplets with ~10^4 electrons was 1% without continuous carrier gas flow (in fact, with 0.07 $L.\,min^{-1}$, this gas flow resulting from the constant pressure operation in the DBD cell maintained using a self-regulating valve located upstream of the pumping system),[43] and is 10% at 0.7 $L.\,min^{-1}$. For larger droplets, the contribution of the neutral drag force becomes even more important. In line with this consideration, the effect of a continuous gas flow rate on droplets transport is examined in more details by light scattering. The results presented in Figure 7 show that in the presence of a continuous gas flow, no light scattering is observed. In sharp contrast with the data set displayed in Figure 4 and added on Figure 7, this suggests that droplets present in the gas gap are less abundant: droplets that remained trapped in the gas gap over multiple low-frequency cycles in the absence of a continuous gas flow are now pushed out of the DBD cell by the neutral drag force.[43]

As in the absence of continuous gas flow described in the previous section, FTIR measurements are also done for the various continuous neutral gas flow rates (Figure 8). At higher continuous flow, an increase of the relative intensity of the Si-$(CH_3)_2$ band can be noticed. As discussed above, this suggests an increase in the degree of plasma polymerization through a methyl

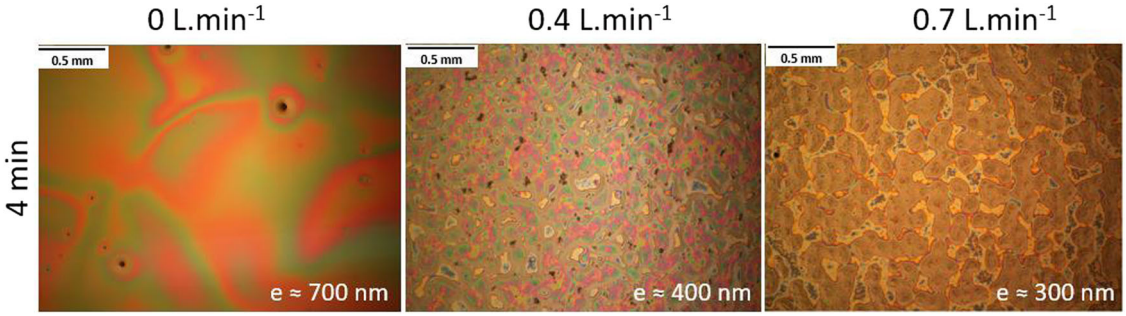

FIGURE 6 Optical images of the deposits obtained after 4 min. for different gas flow conditions.

group removal. A rise in the relative Si-H band intensity at 2250 cm^{-1} can also be seen. In atmospheric-pressure plasma processes, this latter band is the image of the molecular fragmentation of Si-$(CH_3)_3$ such that the Si-H-to-Si-$(CH_3)_3$ band ratio characterizes the molecular fragmentation of the Si-CH_3 and CH bonds.[74] The variation with the continuous gas flow rate thus also reveals different degree of monomer fragmentation with the droplet residence time.

In line with the FTIR analysis performed in Figure 5, Figure 8b displays the influence of the continuous gas flow rate on the Si-$(CH_3)_2$-to-Si-$(CH_3)_3$ band ratio and the position of the Si-O-Si band. Here, the degree of polymerization rises with the flow rate, while the Si-O-Si band position decreases from 1049 to 1043 cm^{-1} between 0 and 1.4 $L.min^{-1}$. Soft polymerization assisted by plasma is thus modified by a continuous nitrogen gas flow, that is, with the droplet residence times.

5 | DISCUSSION

At a given injection rate, that is, with the same type and number of droplets injected in the aerosols, the results obtained in Figures 5 and 8 show that the thin-film morphology and plasma polymerization of HMDSO in a DBD operated in a pulsed direct-liquid-injection mode strongly depends on the deposition parameters, including the deposition time and the droplet residence time. This latter aspect is examined in more details by plotting the degree of plasma polymerization linked to the Si-$(CH_3)_2$-to-Si-$(CH_3)_3$ band ratio and the Si-O-Si band position as a function of the energy parameter (also called by some authors specific energy input (SEI))[16] that can be defined as $E = P \times t_{residence}$, where P is the power determined from electrical analysis of the DBD and $t_{residence}$ is the average time during which the gas remains in the discharge (calculated based on the dimensions of the inter-dielectric space and the continuous N_2 gas flow rate).

The results of the correlation are shown in Figure 9. Here, the set of data (full squares) comes from the FTIR

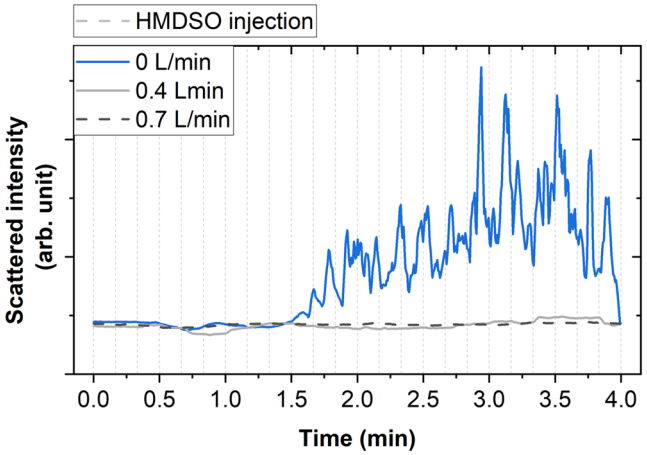

FIGURE 7 Temporal evolution of the intensity of light scattered at 90° with respect to the laser beam for experiments done without various continuous gas flow rate, from 0 to 0.7 L. min^{-1}

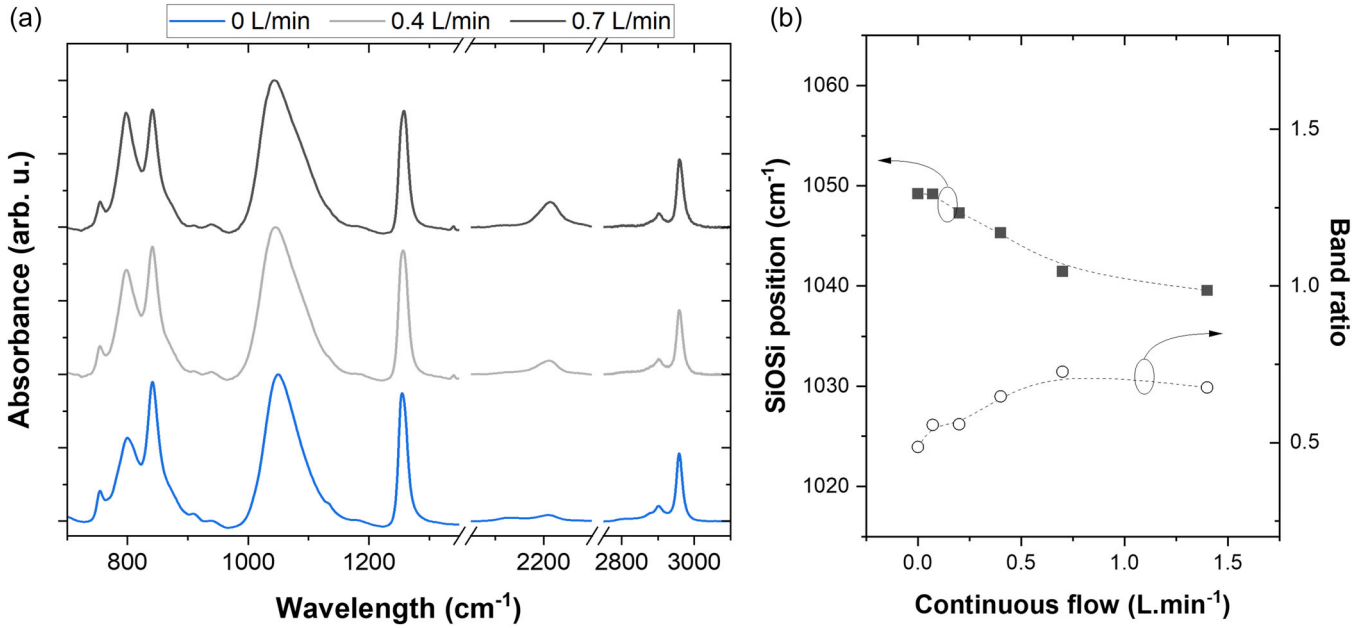

FIGURE 8 (a) FTIR spectra taken in the middle of the sample for various continuous flow at 4 min (b) on the left scale Si-O-Si peak position and on the right scale degree of polymerization (Si-$(CH_3)_2$-to-Si-$(CH_3)_3$ band ratio) as a function of continuous flow

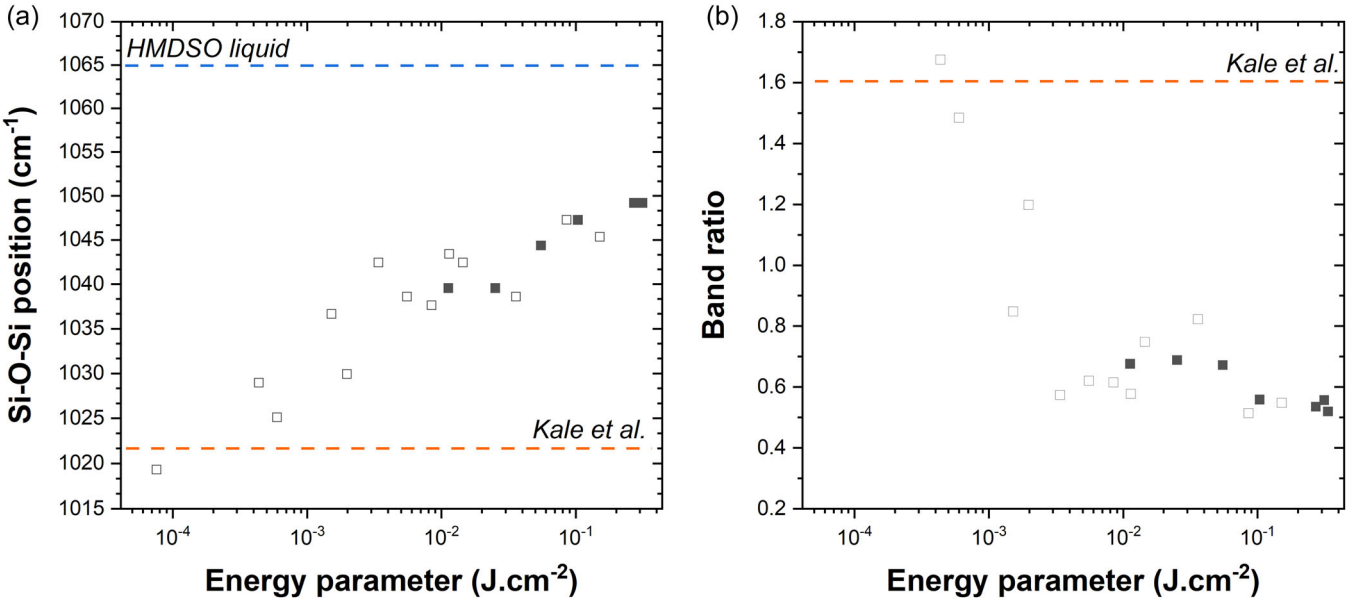

FIGURE 9 (a) Variation of the Si-O-Si peak position and (b) Si-$(CH_3)_2$-to-Si-$(CH_3)_3$ band ratio recorded for a total process time of 4 min as a function of the energy parameter obtained for various plasma deposition times and continuous carrier gas flow rates (full squares). Pulsed injection time of 10 ms, pulsed injection frequency of 0.1 Hz. The results are also shown for various plasma-on times and delay times between precursor injection and plasma ignition with or without a continuous N_2 gas flow (empty square). Orange and blue lines correspond to values for liquid hexamethyldisiloxane (HMDSO) (without plasma polymerization) and plasma-polymerized organosilicon coatings with fully vaporized HMDSO (Kale et al.).[56]

plots after 4 min of deposition as in Figure 8 (influence of continuous nitrogen gas flow rate). Data obtained in a previous study dealing with the effects of other process parameters, namely, duty cycle, delay between precursor injection and discharge ignition, and the amount of injected HMDSO microdroplets are also reported (open squares) for comparison.[43] Clearly, in every condition, a shift in the position of the Si-O-Si peak is observed, from 1020 cm^{-1} at low energy parameter values to 1050 cm^{-1} at higher energies, that is, between the ones of plasma-polymerized organosilicon coatings with fully vaporized HMDSO (as obtained by Kale et al.)[56] to liquid HMDSO,[57] respectively. While vapor-based deposition processes typically reveal significant precursor fragmentation and high degree of cross-linking,[8,56,73] the use of pulsed direct liquid injections at high specific input energies thus offers soft polymerization assisted by plasma with minor fragmentation of the monomer,[57,73] as typically reported in free-radical polymerization.[75] Such a finding is contrary to the intuition as one would expect soft polymerization to occur at low and not at higher energy conditions.

In a previous paper, it was shown that thin-film deposition rates with DLIs coupled to a DBD are limited by the amount of energy provided to precursor droplets, and not by precursor insufficiency.[43] More specifically, the thickness of the deposited film for a total process duration of 4 min. (linked to the deposition rate) increased linearly with the specific energy input. By comparing these findings with the one displayed in Figure 9, it seems that low-energy conditions associated to low thin-film deposition rates are linked to high fragmentation of the monomer. On the other hand, high-energy conditions characterized by high deposition rates yield to soft polymerization assisted by plasma. This conclusion is in sharp contrast to typical vapor-phase plasma deposition for which higher specific energy inputs induce enhanced deposition rates, significant plasma polymerization, and high degrees of cross-linking.[72] With liquid injection, higher thin-film deposition rates are therefore matched with viscous matter.

In our case, the presence of the Si-$(CH_3)_2$ group, considered a chain propagator as in the polydimethylsiloxane, is indicative of the formation of long chains of organosilicon material. In contrast, in vapour-phase deposition as reported by many authors,[8,56,73] the film does not consist of long and isolated Si-O-Si chains, but there is also interchain connections appearing by Si-Si and Si-CH_x cross-linking. In this structure, as illustrated in Figure 10, the –Si-CH_2-Si– bond represents one of the cross-linking points of the long siloxane chains.[76,77] However, the identification of this group in the FTIR spectra is difficult due to the strong absorption in the same wavenumber related to siloxane.[78] Other

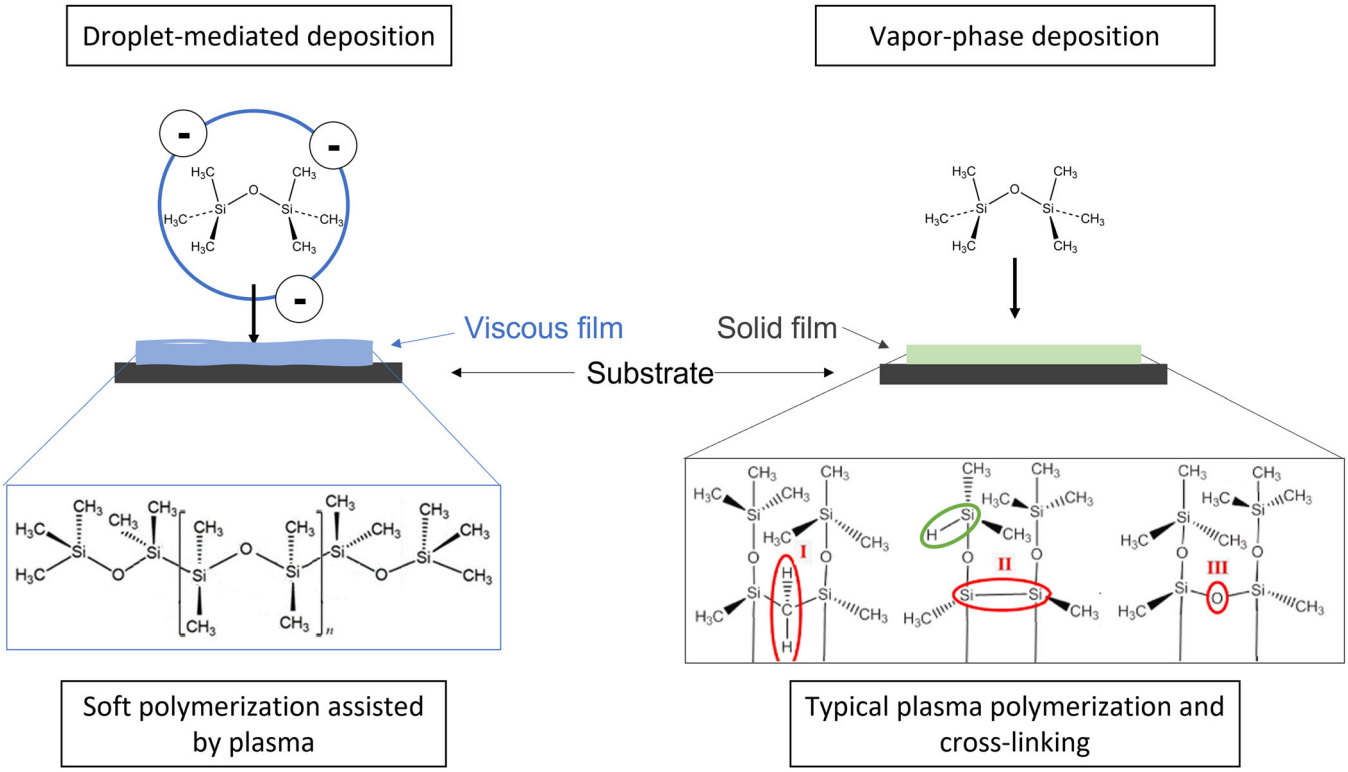

FIGURE 10 Comparison of droplet-mediated and vapor-phase deposition schemes. While droplet-mediated deposition can induce soft polymerization, vapor-phase deposition typically yields plasma polymers with significant cross-linking. In the latter scheme, the Si-CH_2-Si (I), Si-Si (II), Si-O-Si (III) and Si-H (IV) bonds are highlighted because they represent possible points of connection of adjacent chains in organosilicon thin films obtained by plasma polymerization.

possibilities of cross-linking occur by means of the formation of Si-Si and Si-O-Si bonds.[76,77] In all cases, the connection implies the loss of hydrogen atoms and/or methyl groups and hydrogen recombination (Si-H).

On the other hand, for droplet-mediated deposition, FTIR analysis shows that although HMDSO can be dissociated by a methyl group removal in all experimental conditions investigated, only those involving high-deposition rates and the formation of viscous organosilicon films yield to soft polymerization assisted by plasma (Figure 10). In such liquid-phase plasma polymerization conditions, the chemical pathways available for reaction seems much more tightly controlled. In particular, the next highest bond dissociation energy, the C-H bond, is not significantly disrupted by the plasma process (slight modifications of CH_x stretching bands and absence of SiH bands in Figure 5a). Hence, the specific set of plasma conditions appears to deliver sufficient energy to the HMDSO droplets and viscous films to break the weakest monomer bond, thereby enabling the molecule to react and polymerize in the droplet, but without providing the energy required to break higher energy bonds, in particular those leading to Si-CH_2-Si, or any other kind of bridges.[76,77] In short, the monomer is not heavily fragmented, and the process leads to soft polymerization assisted by plasma in liquid droplets with very low cross-linking. At this stage of the study, it is however impossible to distinguish if polymerization occurs in the gas phase through filaments-droplets interactions and/or on the surface through plasma-coating interactions.

6 | CONCLUSION

This study investigates the process of plasma-assisted polymerization by pulsed DLI of HMDSO in a plane-to-plane DBD. The interaction of the plasma with the droplets injected into the interelectrode gap is analyzed, and its effect on the deposition process is assessed. The effects of deposition time and droplet residence time on the characteristics of the deposited films are also examined. In the absence of a continuous carrier gas flow rate, it is shown that the morphology and the degree of precursor fragmentation evolve during the deposition process due to the confinement of charged droplets in the inter-dielectrics space. The plasma-droplet interactions and the nature of the plasma-deposited material can be further controlled by varying the carrier gas

flow conditions. In general, the droplets injected into a DBD are subject to three main processes: droplet charging inside the plasma, deposition of small droplets by the low-frequency electrical field, and the escape of large droplets being confined in the gas gap and then being pushed out of the DBD cell by the neutral drag force. In contrast to typical vapor-phase deposition methods, the use of pulsed DLI offers both enhanced thin-film deposition rates and original polymerization at high specific energy inputs. In such conditions, the plasma can deliver sufficient energy to the HMDSO droplets and viscous films to break the weakest monomer bond, thereby enabling the molecule to react and polymerize but without providing the energy required to break higher energy bonds. Judicious control of vapor and liquid phases injected in plasmas thus seems crucial for soft polymerization assisted by plasma and (multi)functional thin film deposition.

ACKNOWLEDGMENTS

This work was financially supported by the Université Toulouse III - Paul-Sabatier, the CNRS, and the Direction des Relations Internationales of the Université de Montréal through their contributions to the Québec-France International Research Network on Nanomatériaux Multifonctionnels Contrôlés (IRN-NMC).

DATA AVAILABILITY STATEMENT

The data are available from the corresponding author upon request. Data openly available in a public repository that issues data sets with DOIs.

ORCID

Luc Stafford https://orcid.org/0000-0003-0647-543X
Richard Clergereaux https://orcid.org/0000-0001-8014-6154

REFERENCES

[1] Z. Machala, M. Janda, K. Hensel, I. Jedlovský, L. Leštinská, V. Foltin, V. Martišovitš, M. Morvová, *J. Mol. Spectrosc.* **2007**, *243*(2), 194.
[2] I. R. Durán, J. Profili, L. Stafford, G. Laroche, *Mater. Chem. Phys.* **2020**, *242*, 122508.
[3] J. Vallade, S. Pouliquen, P. Lecouvreur, R. Bazinette, E. Hernandez, S. Quoizola, F. Massines, *Energy Procedia* **2012**, *27*, 365.
[4] J. Profili et al., *ACS Sustain. Chem. Eng.* **2020**, *8*(12), 4728.
[5] S. Asadollahi, M. Farzaneh, L. Stafford, *Coatings* **2019**, *9*(10), 679.
[6] R. Jafari, G. Momen, E. Eslami, *Surf. Eng.* **2019**, *35*(5), 450.
[7] F. Fanelli, A. M. Mastrangelo, G. Caputo, F. Fracassi, *Surf. Coat. Technol.* **2019**, *358*, 67.
[8] J. Bour, J. Bardon, H. Aubriet, D. Del Frari, B. Verheyde, R. Dams, D. Vangeneugden, D. Ruch, *Plasma Processes Polym.* **2008**, *5*(8), 788.
[9] D. Merche, N. Vandencasteele, F. Reniers, *Thin Solid Films* **2012**, *520*(13), 4219.
[10] F. Massines, C. Sarra-Bournet, F. Fanelli, N. Naudé, N. Gherardi, *Plasma Processes Polym.* **2012**, *9*(11–12), 1041.
[11] F. Fanelli, *Surf. Coat. Technol.* **2010**, *205*(5), 1536.
[12] A. Uricchio, F. Fanelli, *Processes* **2021**, *9*(11), 2069.
[13] S. Babaei, J. Profili, S. Asadollahi, A. Sarkassian, A. Dorris, S. Beck, L. Stafford, *Plasma Processes Polym.* **2020**, *17*(12), 2000091.
[14] I. Vinogradov, A. Lunk, *Plasma Processes Polym.* **2009**, *6*(S1), S514.
[15] B. Nisol, J. Ghesquière, F. Reniers, *Plasma Chem. Plasma Processes.* **2016**, *36*(5), 1239.
[16] D. Hegemann, E. Bülbül, B. Hanselmann, U. Schütz, M. Amberg, S. Gaiser, *Plasma Processes Polym.* **2021**, *18*(2), 2000176.
[17] A. J. Choudhury, J. Chutia, H. Kakati, S. A. Barve, A. R. Pal, N. S. Sarma, D. Chowdhury, D. S. Patil, *Vacuum* **2010**, *84*(11), 1327.
[18] O. Levasseur, L. Stafford, N. Gherardi, N. Naudé, V. Blanchard, P. Blanchet, B. Riedl, A. Sarkissian, *Plasma Processes Polym.* **2012**, *9*(11–12), 1168.
[19] D. Loffhagen, M. M. Becker, D. Hegemann, B. Nisol, S. Watson, M. R. Wertheimer, C. Klages, *Plasma Processes Polym.* **2020**, *17*(2), 1900169.
[20] R. A. Siliprandi, S. Zanini, E. Grimoldi, F. S. Fumagalli, R. Barni, C. Riccardi, *Plasma Chem. Plasma Process.* **2011**, *31*(2), 353.
[21] R. Magnan, R. Clergereaux, C. Villeneuve-Faure, B. Lantin, G. Carnide, P. Raynaud, N. Naude, *Eur. Phys. J. Appl. Phys.* **2022**, *97*, 37.
[22] K. Lukaszkowicz, *Review of Nanocomposite Thin Films and Coatings Deposited by PVD and CVD technology*, Intech, Rijeka **2011**, pp. 145.
[23] D. Ogawa, I. Saraf, A. Sra, R. Timmons, M. Goeckner, L. Overzet, *J. Vac. Sci. Technol., A* **2009**, *27*(2), 342.
[24] S. Chouteau, M. Mitronika, A. Goullet, M. Richard-Plouet, A. Granier, L. Stafford, *J. Phys. D-Appl. Phys.* **2022**.
[25] M. C. Vasudev, K. D. Anderson, T. J. Bunning, V. V. Tsukruk, R. R. Naik, *ACS Appl. Mater. Interfaces* **2013**, *5*(10), 3983.
[26] A. J. Beck, R. D. Short, A. Matthews, *Surf. Coat. Technol.* **2008**, *203*(5–7), 822.
[27] B. Twomey, D. Dowling, G. Byrne, L. O'Neill, L.-A. O'Hare, *Plasma Processes Polym.* **2007**, *4*(S1), S450.
[28] M. Tatoulian, F. Arefi-Khonsari, J.-P. Borra, *Plasma Processes Polym.* **2007**, *4*(4), 360.
[29] P. Heyse, R. Dams, S. Paulussen, K. Houthoofd, K. Janssen, P. A. Jacobs, B. F. Sels, *Plasma Processes Polym.* **2007**, *4*(2), 145.
[30] F. Fanelli, S. Lovascio, R. d'Agostino, F. Fracassi, *Plasma Processes Polym.* **2012**, *9*(11–12), 1132.
[31] E. Nadal, N. Milaniak, H. Glenat, G. Laroche, F. Massines, *Nanotechnology* **2021**, *32*(17), 175601.
[32] M. Mitronika, J. Profili, A. Goullet, N. Gautier, N. Stephant, L. Stafford, A. Granier, M. Richard-Plouet, *J. Phys. D Appl. Phys.* **2020**, *54*(8), 085206.
[33] M. Mitronika, A. Granier, A. Goullet, M. Richard-Plouet, *SN Appl. Sci.* **2021**, *3*(6), 665.

[34] P. Brunet, R. Rincón, J. Margot, F. Massines, M. Chaker, *Plasma Processes Polym.* **2017**, *14*(7), 1600075.
[35] A. Uricchio, E. Nadal, B. Plujat, G. Plantard, F. Massines, F. Fanelli, *Appl. Surf. Sci.* **2021**, *561*, 150014.
[36] G. Carnide et al., "Direct Liquid Reactor Injector of Nanoparticles: a safer-by-design aerosol injection method adapted to nanocomposite thin-film deposition in various plasma-assisted processes," Coatings.
[37] P. A. F. Herbert, L. O'Neill, J. Jaroszyńska-Wolińska, *Chem. Mater.* **2009**, *21*(19), 4401.
[38] L. J. Ward, W. C. E. Schofield, J. P. S. Badyal, A. J. Goodwin, P. J. Merlin, *Chem. Mater.* **2003**, *15*(7), 1466.
[39] L.-A. O'Hare, L. O'Neill, A. J. Goodwin, *Surf. Interf. Anal.* **2006**, *38*(11), 1519.
[40] J. Albaugh, C. O'Sullivan, L. O'Neill, *Surf. Coat. Technol.* **2008**, *203*(5–7), 844.
[41] D. Hegemann, S. Gaiser, *J. Phys. D Appl. Phys.* **2021**, *55*, 173002.
[42] T. Jacobs, R. Morent, N. De Geyter, P. Dubruel, C. Leys, *Plasma Chem. Plasma Process.* **2012**, *32*(5), 1039.
[43] L. Cacot, G. Carnide, M. L. Kahn, R. Clergereaux, N. Naudé, L. Stafford, *J. Phys. D Appl. Phys.* Oct. **2022**, *55*(47), 475202. https://doi.org/10.1088/1361-6463/ac94de
[44] M. Coppins, *Phys. Rev. Lett.* **2010**, *104*(6), 065003.
[45] J. Profili, S. Dap, O. Levasseur, N. Naude, A. Belinger, L. Stafford, N. Gherardi, *J. Phys. D Appl. Phys.* **2017**, *50*(7), 075201.
[46] I. Enache, H. Caquineau, N. Gherardi, T. Paulmier, L. Maechler, F. Massines, *Plasma Processes Polym.* **2007**, *4*(9), 806.
[47] J. Bardon, R. Dieden, P. Grysan, G. Mertz, A. Martin, M. Delmée, D. Ruch, *Surf. Coat. Technol.* **2019**, *358*, 320.
[48] A. Shelemin, A. Choukourov, J. Kousal, D. Slavínská, H. Biederman, *Plasma Processes Polym.* **2014**, *11*(9), 864.
[49] J. Petersen, J. Bardon, A. Dinia, D. Ruch, N. Gherardi, *ACS Appl. Mater. Interf.* **2012**, *4*(11), 5872.
[50] N. D. Mejanes, J. Profili, S. Babaei, N. Naudé, L. Stafford, *J. Phys. D: Appl. Phys.* **2020**, *54*(9), 095204. https://doi.org/10.1088/1361-6463/abcb32
[51] J. Profili, O. Levasseur, N. Naudé, C. Chaneac, L. Stafford, N. Gherardi, *J. Appl. Phys.* **2016**, *120*(5), 053302.
[52] T. C. Manley, *Trans. Electrochem. Soc.* **1943**, *84*(1), 83.
[53] Z. Zhao, Z. Zheng, C. Roux, C. Delmas, J. D. Marty, M. L. Kahn, C. Mingotaud, *Chem. A Eur. J.* **2016**, *22*(35), 12424.
[54] F. Massines, N. Gherardi, A. Fornelli, S. Martin, *Surf. Coat. Technol.* **2005**, *200*(5–6), 1855.
[55] I. Rodríguez Durán, A. Durocher-Jean, J. Profili, L. Stafford, G. Laroche, *Plasma Processes Polym.* **2020**, *17*(7), 1900186.
[56] K. H. Kale, S. Palaskar, *Text. Res. J.* **2011**, *81*(6), 608.
[57] L. O'Neill, P. A. F. Herbert, C. Stallard, D. P. Dowling, *Plasma Processes Polym.* **2010**, *7*(1), 43.
[58] R. Morent, N. De Geyter, S. Van Vlierberghe, P. Dubruel, C. Leys, L. Gengembre, E. Schacht, E. Payen, *Prog. Org. Coat.* **2009**, *64*(2–3), 304.
[59] D. S. Wavhal, J. Zhang, M. L. Steen, E. R. Fisher, *Plasma Processes Polym.* **2006**, *3*(3), 276.
[60] Y.-C. Lin, M.-J. Wang, *Jpn. J. Appl. Phys.* **2018**, *58*(SA), SAAC01.
[61] U. Kogelschatz, *IEEE Trans. Plasma Sci.* **2002**, *30*(4), 1400.
[62] N. Gherardi, G. Gouda, E. Gat, A. Ricard, F. Massines, *Plasma Sources Sci. Technol.* **2000**, *9*(3), 340.
[63] N. Naudé, J.-P. Cambronne, N. Gherardi, F. Massines, *Eur. Phys. J. Appl. Phys.* **2005**, *29*(2), 173.
[64] I. Fortelnỳ, J. Juza, B. Dimzoski, *Eur. Polym. J.* **2012**, *48*(7), 1230.
[65] Q. Sheng, J. Sun, Q. Wang, W. Wang, H. S. Wang, *Sci. Rep.* **2016**, *6*(1), 1.
[66] N. Naudé, J. P. Cambronne, N. Gherardi, F. Massines, *J. Phys. D Appl. Phys.* **2005**, *38*(4), 530.
[67] K.-Y. Li, H. Tu, A. K. Ray, *Langmuir* **2005**, *21*(9), 3786.
[68] E. D. Bennet, C. Mahony, H. E. Potts, P. Everest, D. Rutherford, S. Askari, D. A. McDowell, D. Mariotti, C. Kelsey, F. Perez-Martin, N. Hamilton, P. Maguire, D. A. Diver, *J. Aerosol Sci.* **2016**, *100*, 53.
[69] R. Seco-Gudiña, J. Guadarrama-Cetina, W. González-Viñas, *Eur. Phys. J. Special Top.* **2017**, *226*(6), 1189.
[70] J. Guadarrama-Cetina, W. González-Viñas, *Phys. Rev. E* **2013**, *87*(5), 054401.
[71] W. Ristenpart, P. McCalla, R. Roy, H. A. Stone, *Phys. Rev. Lett.* **2006**, *97*(6), 064501.
[72] C. P. Stallard, M. M. Iqbal, M. M. Turner, D. P. Dowling, *Plasma Processes Polym.* **2013**, *10*(10), 888.
[73] R. Morent, N. De Geyter, S. Van Vlierberghe, P. Dubruel, C. Leys, E. Schacht, *Surf. Coat. Technol.* **2009**, *203*(10–11), 1366.
[74] M. Ricci, J.-L. Dorier, C. Hollenstein, P. Fayet, *Plasma Processes Polym.* **2011**, *8*(2), 108.
[75] H.-G. Elias, *Macromolecules*, Springer, **1977**, pp. 535.
[76] A. S. M. de Freitas, C. C. Maciel, J. S. Rodrigues, R. P. Ribeiro, A. O. Delgado-Silva, E. C. Rangel, *Vacuum* **2021**, *194*, 110556.
[77] R. P. Ribeiro, R. C. C. Rangel, F. O. Fernandes, N. C. Cruz, E. C. Rangel, *Mater. Res.* **2021**, *24*. https://doi.org/10.1590/1980-5373-MR-2021-0039
[78] C. Rau, W. Kulisch, *Thin Solid Films* **1994**, *249*(1), 28.

How to cite this article: L. Cacot, G. Carnide, M. L. Kahn, N. Naudé, L. Stafford, R. Clergereaux, *Plasma. Process. Polym.* **2022**, e2200165. https://doi.org/10.1002/ppap.202200165